Preliminary design method accounting for shape distortion in Metal Binder Jetting parts: a case study

M. Zago[1[0000-0002-2798-5482]], M. Perina[2], I. Cristofolini[1[0000-0003-2787-1271]]

[1] Department of Industrial Engineering, University of Trento, Via Sommarive 9, 38123, Trento – Italy
[2] Mimest Srl, Via del Lavoro 30, 38063, Avio - Italy
marco.zago-1@unitn.it

Abstract. Additive Manufacturing (AM) technologies theoretically allow the production of complex products without any geometrical restriction. Nevertheless, production process delineates some limitations on the resulting dimensional and geometrical precision. This is a critical issue mainly for Metal Binder Jetting (MBJ) process, on the reason of anisotropic dimensional change and distortion on sintering. Literature reports fairly reliable models for predicting the deformation on sintering. However, the application of such methods might be time consuming from industrial perspective, because of the extensive experimental analysis required to assemble a robust material database. For that reason, this work aims at proposing an alternative approach for compensating dimensional and geometrical change on sintering. Two complex geometries, having similar geometrical features with different sizes, were printed and measured by a coordinate measuring machine before and after sintering process. The analysis of cylindricity form errors reveals an excellent geometrical stability of smaller geometry. Therefore, dimensional change along printing direction was derived in order to obtain a precise scaling factor for improving the dimensional and geometrical precision. By contrast, bigger samples encountered a dramatic distortion, which required a complete redesign. The shape of the distorted cylinder was approximated with an ellipse and a corrective function has been proposed for compensating green geometry.

Keywords: Additive Manufacturing, Binder Jetting, Design for AM, distortion.

1 Introduction

Additive Manufacturing (AM) combines several advantages but even weakness points which currently circumscribes a wide industrial application [1]. Among different AM technologies, Binder jetting (BJ) is an interesting and cost-effective AM process on the reason of both the low feedstock price and the high production rate [2, 3]. Starting from 3D CAD file, the product is built up by spreading powder layer and injecting the binder in the region defined by CAD slicing. Repeating these steps, the green product can be printed without warpage and distortion issues, which could happen in powder-bed fusion (PBF) or direct energy deposition (DED) [4]. The main drawback of BJ is related to the secondary operations: debinding and sintering, which are needed to remove binder agent and consolidate metal structure.

The dimensional and geometrical quality of BJ product is highly affected by sintering. Several experimental works report a high volume change on sintering and a higher shrinkage along printing direction than in the printing plane [5, 6]. There is also evidence of slightly higher shrinkage along printing head movement direction with respect to powder spreading direction [7]. In addition to anisotropic shrinkage, literature reports some examples of distortion in sintered MBJ products. Zhang et al experimentally analyzed dimensional and geometrical deformation of overhanging geometries as cantilever and bridge samples [8]. Experimental data and simulation models demonstrate the influence of both gravity load and visco-plastic behavior of material during heating. The visco-plastic behavior is not the unique cause of distortion on sintering. Lee et al. numerically demonstrate that distortion can be also originated by inhomogeneity in local density of green part [9]. In fact, a gradient of density implies different shrinkage intensity, which could originate deformation.

Literature clearly demonstrates the complexity of distortion prevision on MBJ. Zhang et al. highlighted the absence of a material database, which can be used by designers [8]. The development of material database is challenging for the future development of a design method for Additive Manufacturing (DfAM). However, the material characterization might be time consuming from industrial perspective, which needs for design guidelines ready to use. For that reason, this work aims a proposing a design approach for compensating sintering deformation. Two geometries, connectors having similar shape and different sizes, were printed using AISI 316L gas atomized metal powders. The parts were successively measured both at green and sintered state by a Coordinate Measuring Machine (CMM). The measurements highlighted a very good stability of the smaller parts and an extremely high distortion in the bigger connectors. A corrective function has been proposed for compensating the green geometry in the last case.

The outline of the paper is organized as follows. Section 2 describes the experimental procedure and the model for assessing a corrective function of shape distortion. Section 3 discusses the dimensional and geometrical change on sintering, in addition to the tuning of the corrective function. Finally, the conclusion summarizes the results and further perspective.

2 Method and Model

AISI 316L gas atomized powder has been employed in this work. Two different sample geometries were printing by a Digital Metal printing machine (P1701) according to the process parameters defined in Table 1.

Table 1. Printing parameters.

Layer thickness	Resolution	Bed temperature	Printing speed
42 μm	1200 dpi	80°C	200 mm/s

Fig. 1 shows the axonometric view of the two geometries and the printing reference system.

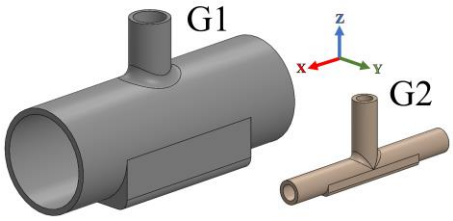

Fig. 1. Axonometric view of the connectors – geometry 1 – G1 and geometry 2 – G2.

Four replicates were printed for each geometry in a single batch in order to check repeatability. The nominal geometries were scaled according to the scale factor provided by machine supplier, and successively the CAD files were converted to STL files imposing a deviation and angle tolerance of 0.0014 mm and 0.5°, respectively. By this way, the tessellation of STL file would not affect the precision of geometry, more significantly affected by staircase error of layer-by-layer manufacturing.
In the printing chamber, all samples were aligned according to Fig. 1. The axis of horizontal cylinder (cylinder A) was oriented parallel to the X direction, which corresponds to the binder spreading direction, whereas the axis of vertical cylinder (cylinder B) was aligned along Z printing direction, which corresponds to the building direction.

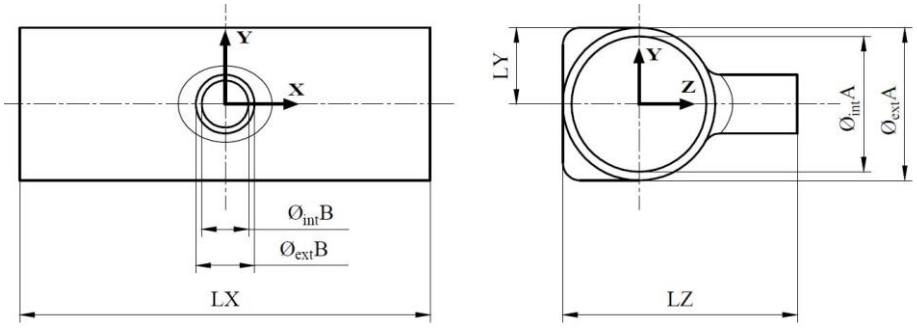

Fig. 2. Drawing of geometry 1 and conventional name of the main dimensions investigated. Same convention is adopted for geometry 2.

Table 2 reports the parametric nominal dimensions of sintered products, referring to the dimensions displayed in Fig. 2. Dimensions were parametrized with respect to a factor *w* in order to preserve the design characteristics.

Table 2. Nominal dimensions of the two sample connectors. Dimension labels are defined according to Fig. 2.

Geometry	ϕ_{ext}A [mm]	ϕ_{int}A [mm]	ϕ_{ext}B [mm]	ϕ_{int}B [mm]	LX [mm]	LY [mm]	LZ [mm]
G1	6.5 *w*	5.75 *w*	2.5 *w*	2 *w*	17.5 *w*	3.25 *w*	10 *w*
G2	1.5 *w*	*w*	1.5 *w*	*w*	12.5 *w*	1.5 *w*	5 *w*

After printing process, the dimensional and geometrical characteristics of green samples were measured by a coordinate measuring machine (CMM). Hexagon Global image 07-07-07 CMM has been used mounting a Renishaw SP600M touch-probe which has a maximum permissible error of 1.5 +L/333 μm in touching acquisition mode according to ISO 10360-2. The axis of cylinder A was used for the definition of X direction of the reference system, whereas the axis of cylinder B identifies Z axis. Moreover, the intersection of the axes determined the origin of the Datum Reference Frame (DRF).

The measurement has been performed by touching acquisition mode in order to prevent the scratching of green part surface, which could occur using continuous scanning mode. The measurement procedure was coded by Pc-dmis 2021R2 suite. Basically, the procedure consisted of manual alignment followed by a more precise automatic alignment. Successively, points were acquired on the flat surfaces, which are the base planes of the cylinders in order to reconstruct the linear dimensions by plane distance. Referring to the linear dimensions, the external and internal diameter of cylinder B were scanned at three different levels parametrically defined according to linear dimension. The external and internal diameter of cylinder A were scanned at six levels, three on the left and three on the right with respect to the axis of cylinder B, as shown in Fig. 3.

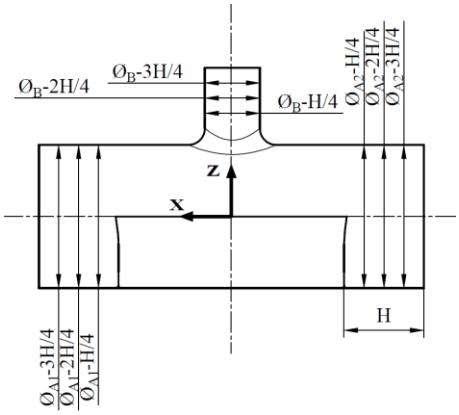

Fig. 3. Conventional names of the circles measured at different depth on cylinders A and B with respect to the DRF.

For each circle measurement, 24 points were acquired around the circumference at equidistant angular positions. By these points, internal and external cylinders were reconstructed by best fit least square method.

The green samples were then thermally debinded at 640°C in a continuous furnace, before sintering at the isothermal temperature of 1385°C for 210 minutes.

Sintered samples were measured according to the same procedure developed for green parts. Since geometry 1 showed a high distortion, the points on the base planes of cylinder A were acquired manually in order to define the linear dimensions. Circle measurements have been performed automatically by the same procedure developed for green parts.

By experimental data, the linear dimensional change on sintering (ε_L) was computed by the normalized difference between sintered ($l_{sintered}$) and green (l_{green}) dimensions, as reported in equation (1):

$$\varepsilon_L = \frac{l_{sintered} - l_{green}}{l_{green}} \tag{1}$$

The geometrical stability of cylinder on sintering was evaluated by cylindricity form errors. Moreover, shape distortion was analyzed locally, evaluating the fitting the points measured at different levels. The points measured on each circle of cylinder A (geometry 1) were fitted by equation (2) in order to analyze the influence of depth levels on distortion.

$$\frac{[(y-y_0)\cos\theta+(z-z_0)\sin\theta]^2}{a^2} + \frac{[(y-y_0)\sin\theta-(z-z_0)\cos\theta]^2}{b^2} = 1 \tag{2}$$

Where:

— y_0 and z_0 are the coordinates of the intersection of ellipse's axes;
— a is the major semi axis of the ellipse;
— b is the minor semi axis of the ellipse;
— θ is the ellipse rotation angle around X axis.

Looking for a corrective function of the cylinder distortion, the profile of the derived ellipse was express in polar coordinates by equation (3).

$$R_{ellipse}(\alpha) = \sqrt{y(\alpha)^2 + z(\alpha)^2} \tag{3}$$

Where α is the free angular variable ranging from 0 to 2π, whereas $y(\alpha)$ and $z(\alpha)$ coordinates can be derived by the ellipse parameters according to equations (4) and (5), respectively.

$$y(\alpha) = a\cos\alpha\cos\theta - b\sin\alpha\sin\theta + y_0 \tag{4}$$

$$z(\alpha) = a\cos\alpha\sin\theta + b\sin\alpha\cos\theta + z_0 \tag{5}$$

The above coordinate system allowed to compute the difference between the polar coordinate of the elliptic shape and the desired nominal geometry (R_{circle}), as defined by equation (6).

$$\text{Distance}(\alpha) = R_{ellipse}(\alpha) - R_{circle} \tag{6}$$

The difference between deformed and nominal shape was finally fitted by a sinusoidal equation expressed by equation (7), in order to provide an analytical equation to be used for correcting the geometry of the green part.

$$f(\alpha) = Amp * \sin(2\pi * f * \alpha + \psi) + y_{offset} \tag{7}$$

Where:

— Amp is the amplitude of the sinusoidal function;

– f is the frequency;
– α is the free angular variable which ranges from 0 to 2π;
– ψ is the phase shift;
– y_{offset} is the offset of the sinusoidal function with respect to Y axis.

3 Results and discussion

The geometry of cylinders was evaluated according to the cylindricity form error. Fig. 4 shows the cylindricity form error at green and sintered state, respectively.

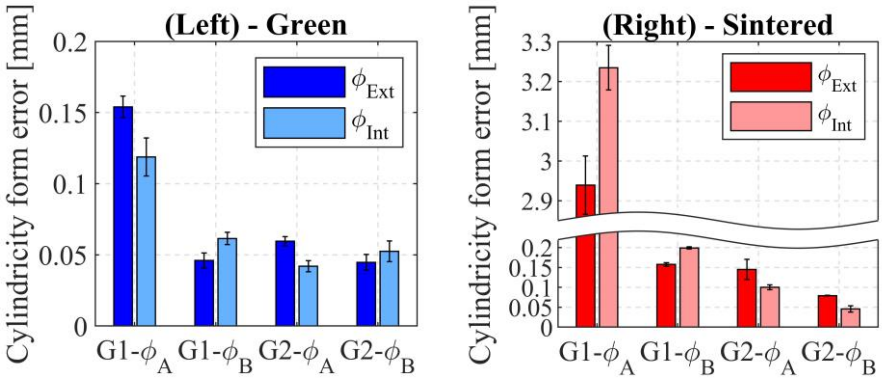

Fig. 4. Cylindricity form error of green (Left) and sintered (Right) samples.

Data in Fig. 4 do not show any clear trend ascribable to external/internal features, neither at green state (Fig. 4-Left), nor at sintered state (Fig. 4-Right).

Concerning geometry 1, at green state cylinder A displays a markedly higher error than cylinder B, likely due to the larger size. At the sintered state, the form error of cylinder A is exceptionally high due to distortion. Since the axis of cylinder B is parallel to the printing direction, a marginal increase of form error was expected. The increase of form error is yet remarkable, and it could be a side effect of the distortion of the supporting cylinder A.

Analyzing the data of geometry 2, at green state cylindricity form errors are in a close range around 0.05 millimeters, as observed in [10]. At sintered state, the form error of cylinder B is substantially the same, while the value related to cylinder A increased. As explained in [10, 11], these results can be directly associated to the higher shrinkage along Z direction than in X-Y directions, which causes a deformation of the circular section of circle.

As closing remark, the small form error highlighted in geometry 2 is determined by anisotropic dimensional change on sintering. Therefore, the geometry is appropriate for MBJ process, since the dimensional and geometrical precision of sintered product can be guaranteed properly tuning the scaling factors to be applied to the green geometry. Conversely, geometry 1 displays an extremely high shape deformation, which is determined by both the gravity-load and the visco-plastic behavior of material activated at

high temperature. For this reason, the geometry of the green part must be redesigned in order to compensate sintering deformation.

The shape distortion of cylinder A (geometry 1) is clearly visible in Fig. 5-Left. Fig. 5-Right shows the measured points acquired at different scan depth along with the nominal external and internal diameters. In addition, Fig. 5-Right displays the ellipses best-fitting the points measured on the external and internal features.

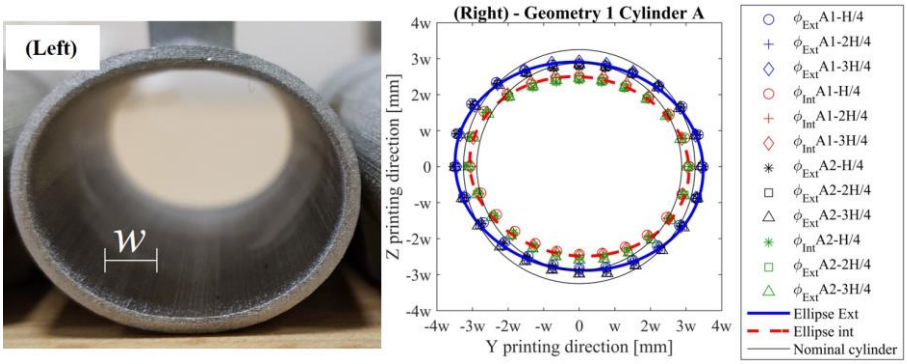

Fig. 5. (Left) Picture showing the shape distortion of cylinder A (geometry 1). (Right) Points measured at different scan depth and ellipses best-fitting the points measured on the external and internal features of cylinder A (geometry 1).

Gravity-load and the visco-plastic behavior of material could have provoked the cylinder deformation due to the high diameter to thickness ratio, determining a slender structure with respect to the overhanging structure.

To better understand the deformation of the sample, the measured points at each of the six levels on cylinder A were fitted by equation (2), and the parameters of the ellipses were analyzed as a function of the depth levels. Fig. 6-Left illustrates the ratio between the minor and major semi-axes of the ellipses derived from the points measured on the internal and external features. Fig. 6-Right shows the ellipse rotation angle around X axis.

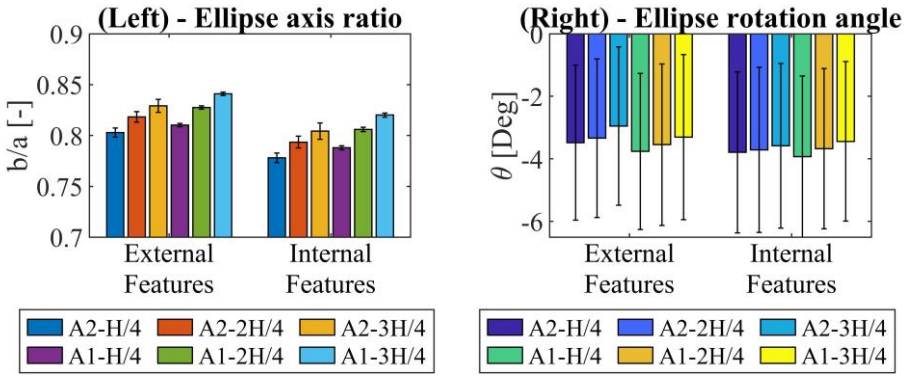

Fig. 6. (Left) Ratio between the minor and major semi-axis of the fitted ellipses at different depth levels of cylinder A (geometry 1). (Right) Rotation angle of the best-fit ellipse at different depth level of the cylinder A. Scatter bands equal to 1 sigma.

Comparing Fig. 3 and Fig. 6-Left, axis ratio increases approaching the edges of the deformed cylinder A, thus meaning a higher distortion at deeper levels, close to the cylinder B. Fig. 6-Right indicates the presence of a moderate rotation of the ellipse axes around X printing direction. A fair trend can be observed with respect to the depth levels, though the scatter band is quite high. Both the trend of axis ratio and tilting angle might be attributed to the curvature of the bottom plane shown in Fig. 7.

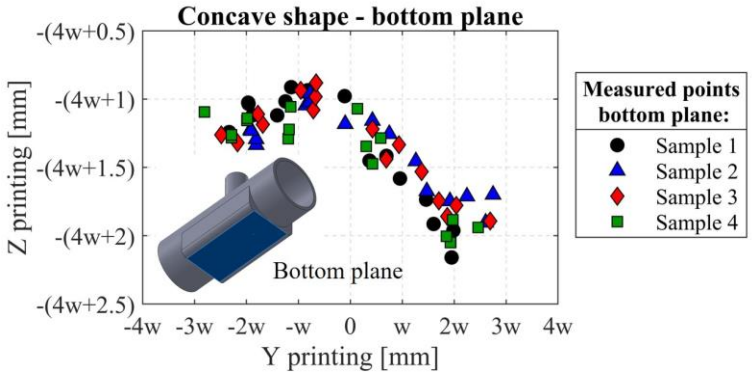

Fig. 7. Y-Z view of the measurement points acquired on the bottom plane of the base support.

As plotted in Fig. 7, the points acquired in the bottom plane of the base support depict a concave shape. Therefore, the deformation of the plane could have induced the higher axis ratio of inner sections on the reason of the higher stiffness of the support, compared to the cylinder. Moreover, the curvature of the plane is not symmetric since there is a more pronounced rotation around Y printing direction, and the bottom plane rotation is consistent with the ellipse rotation shown in Fig. 6-Right.

The reason of the plane deformation is not completely understood. One hypothesis might be related to the particle segregation during powder spreading. The discrete

element analysis of Lee et al [12] suggests that finer particles tend to accumulate in the first layers and consequently the mean particle size distribution shifts towards sample height. According to this hypothesis, the base support (lower layer → smaller particle) could have encountered higher dimensional change than the cylinder (higher layer → bigger particle), provoking the curvature observed in Fig. 7. Another possible explanation involves the friction between the base support and the trays used in the furnace during sintering. Further studies should explore both aspects in order to prevent this distortion.

Fig. 6-Left also indicates a significant difference in the axis ratio in the left and right side of cylinder A. The reason is under investigation. A first hypothesis concerns the influence of the sample position in the printing bed. Lores et al report the presence of inhomogeneity in the powder bed density in the working plane [13]. Future work will investigate the influence of the position in the printing bed on the green density and dimensional change on sintering.

Looking for a corrective function of cylinder shape, the difference between the elliptic profile and nominal circle was calculated according to equation (6). The resulting data of sample 1 (geometry 1) are plotted in Fig. 8 for external and internal features, respectively.

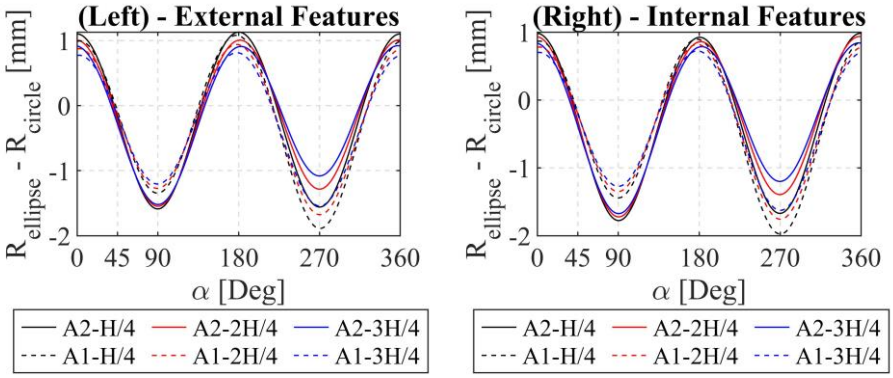

Fig. 8. Sample 1 - geometry 1: difference between the radius of the ellipse and the radius of the circle. (Left) external feature, (Right) internal feature.

Fig. 8 shows a sinusoidal trend which differs as a function of the depth levels and the scan side (section A1 and A2). The non-constant sinusoidal behavior is related to the tilting angle already described, but the position of the ellipse with respect to the axis of the nominal cylinder also plays a significant role. The coordinates of the point resulting from intersection of ellipse's axes are shown in Fig. 9.

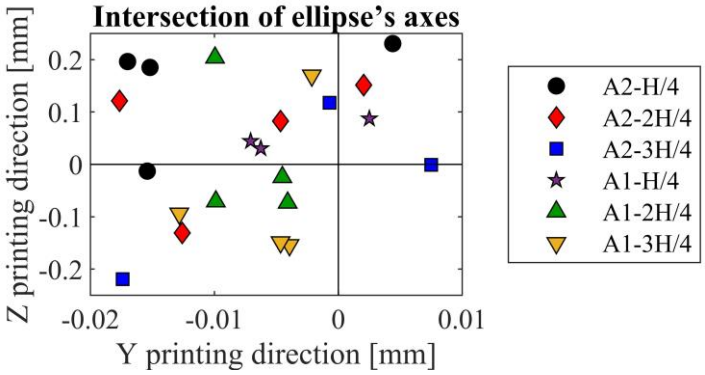

Fig. 9. y_0 and z_0 coordinates of the point derived from the intersection of the ellipse's axes at different depth levels.

In Fig. 9 the points representing the intersection of the ellipse's axes are significantly scattered along Z direction, while y_0 position is mainly located at negative coordinates. The above scatter considerably affects the definition of a corrective function for the overall cylinder section, since different shape correction seems to be needed at different depth levels. A preliminary attempt was conducted fitting the experimental data obtained for each circle measurements of different samples with equation (7). The mean value and standard deviation of the four fitting parameters are reported in Table 3, as well as the Mean Squared Error (MSE).

Table 3. Mean and standard deviation of the parameters of equation (7) derived by fitting the difference between the radius of the ellipse and the circle at all depth levels of four samples.

	Amp [mm]	f [-]	ψ [rad]	y_{offset} [mm]	MSE
Mean	1.284	0.006	1.573	-0.232	0.008
Std. Dev.	0.086	0.000	0.013	0.064	0.006

Data table highlights that amplitude and offset are significantly affected by the scatter of the position of ellipse's axes intersection and tilting angle. In addition the mean MSE is virtually low, however the standard deviation is comparable on the reason of different sinusoidal behavior at different depth levels. In future work, the geometry of cylinder A will be corrected according to the derived function. However, further refinements are required to reduce any gradient in green density, which is likely the cause for distortion discrepancy at different printing position.

In conclusion the dimensional change on sintering is reported in Table 4. Regarding geometry 1, the dimensional changes reported do not exclusively depend on material densification on sintering. In fact, distortion markedly affected both diameter and linear dimensions, and specifically no diameter could be recognized after sintering in the feature derived from cylinder A (so that corresponding values in Table 4 are missing). Conversely, geometry 2 does not display distortion. In fact, the dimensional change of both diameter and linear dimensions are in a close range. As expected, the linear

shrinkage of LZ is higher in comparison with dimensional changes in the printing plane, as widely reported in literature [5–7]. Data in table 4 show a slightly higher shrinkage of internal diameter than external one, both for cylinder A and B, to be further investigated.

Finally, it is important to observe that standard deviation is in a close range, in comparison with mean dimensional change. This demonstrates a good repeatability of the process in order to produce precise parts.

Table 4. Mean and standard deviation of the dimensional change on sintering of diameter and linear dimensions.

Geometry	ϕ_{ext}A mean (d.st) [%]	ϕ_{int}A mean (d.st) [%]	ϕ_{ext}B mean (d.st) [%]	ϕ_{int}B mean (d.st) [%]	LX mean (d.st) [%]	LY mean (d.st) [%]	LZ mean (d.st) [%]
G1	/	/	-17.87 (0.42)	-18.58 (0.45)	-17.37 (0.22)	22.26 (2.96)	-14.32 (0.17)
G2	-17.85 (0.41)	-19.22 (0.12)	-17.95 (0.19)	-19.10 (0.21)	-17.54 (0.11)	-17.34 (0.38)	-19.46 (0.08)

4 Conclusions

The present work analyzes the feasibility of metal binder jetting process producing complex shape parts. Two similar geometries were chosen, having the same geometrical features with different sizes. Four replicates for each geometry were printed in the same batch using AISI 316L gas atomized powder. Samples were then measured by a coordinate measuring machine before and after the sintering process in order to evaluate the dimensional and geometrical changes on sintering.

The results show:

- Geometry 2 (smaller size): small form error both at green and sintered state. Therefore, the geometry seems affordable for mass production, provided that properly tuned scaling factors are applied to green geometry in order to compensate the anisotropic shrinkage on sintering.
- Geometry 1 (bigger size): large distortion during sintering, likely due to the gravity-load and the visco-plastic behavior of the material at high temperature. The observed distortion implies that the geometry needs to be completely redesigned in order to correct the deformation occurred on sintering.
- The distorted shape was reconstructed fitting the measured points by elliptic function. The analysis of the fitting parameters describes a non-homogenous distortion along cylinder depth, likely due to the influence of the deformation of the base support.
- A parametric corrective function has been proposed to correct the distorted geometry. The proposed sine function was derived by fitting the difference between the radial coordinate of the ellipse and the nominal sintered geometry, as a function of the angular position.

As a final remark, this work highlights the affordability of producing complex geometries with small size, comparable with the size of standard MIM products. On increasing the product size, the precision can be detrimentally affected by sintering deformation due to the visco-plastic behavior of the material and/or by the inhomogeneity in powder bed density. In such conditions, the geometry of the product has to be completely redesigned. Further investigation will identify the process parameters mostly affecting the deformation on sintering, to be considered in effective design guidelines for part producers.

References

1. Bacciaglia, A., Ceruti, A., Liverani, A.: Additive Manufacturing Challenges and Future Developments in the Next Ten Years. In: Lecture Notes in Mechanical Engineering. pp. 891–902. Springer International Publishing (2020).
2. Ziaee, M., Crane, N.B.: Binder jetting: A review of process, materials, and methods. Addit. Manuf. 28, 781–801 (2019).
3. Li, M., Du, W., Elwany, A., Pei, Z., Ma, C.: Metal Binder Jetting Additive Manufacturing: A Literature Review. J. Manuf. Sci. Eng. 142, 1–17 (2020).
4. Song, X., Feih, S., Zhai, W., Sun, C.N., Li, F., Maiti, R., Wei, J., Yang, Y., Oancea, V., Romano Brandt, L., Korsunsky, A.M.: Advances in additive manufacturing process simulation: Residual stresses and distortion predictions in complex metallic components. Mater. Des. 193, 108779 (2020).
5. Ziaee, M., Tridas, E.M., Crane, N.B.: Binder-Jet Printing of Fine Stainless Steel Powder with Varied Final Density. Jom. 69, 592–596 (2017).
6. Lecis, N., Mariani, M., Beltrami, R., Emanuelli, L., Casati, R., Vedani, M., Molinari, A.: Effects of process parameters, debinding and sintering on the microstructure of 316L stainless steel produced by binder jetting. Mater. Sci. Eng. A. 828, 142108 (2021).
7. Cabo Rios, A., Hryha, E., Olevsky, E., Harlin, P.: Sintering anisotropy of binder jetted 316L stainless steel: part I – sintering anisotropy. Powder Metall. 0, 1–10 (2021).
8. Zhang, K., Zhang, W., Brune, R., Herderick, E., Zhang, X., Cornell, J., Forsmark, J.: Numerical simulation and experimental measurement of pressureless sintering of stainless steel part printed by Binder Jetting Additive Manufacturing. Addit. Manuf. 47, 102330 (2021).
9. Lee, Y., Nandwana, P., Simunovic, S.: Powder spreading, densification, and part deformation in binder jetting additive manufacturing. Prog. Addit. Manuf. (2021).
10. Zago, M., Lecis, N.F.M., Vedani, M., Cristofolini, I.: Dimensional and geometrical precision of parts produced by Binder Jetting process as affected by the anisotropic shrinkage on sintering. Addit. Manuf. (2021).
11. Zago, M., Lecis, N.F.M., Vedani, M., Cristofolini, I.: Geometrical Issues in Design for Binder Jetting - The Effect of Anisotropic Dimensional Change on Sintering. In: Design Tools and Methods in Industrial Engineering II. pp. 410–421 (2022).
12. Lee, Y., Gurnon, A.K., Bodner, D., Simunovic, S.: Effect of Particle Spreading Dynamics on Powder Bed Quality in Metal Additive Manufacturing. Integr. Mater. Manuf. Innov. 9, 410–422 (2020).
13. Lores, A., Azumendi, N., Agote, I., Andres, U.: A step towards a robust binder jetting technology: Process parameter optimization for 17-4 PH steel to increase powder bed homogeneity. Procedings Eur. 2020 Int. Powder Metall. Virtual Congr. Exhib. (2020).